# Formation of a N^2-dG:N^2-dG Carbinolamine DNA Cross-link by the trans-4-Hydroxynonenal-Derived (6S,8R,11S) 1,N^2-dG Adduct

Hai Huang, Hao Wang, Albena Kozekova, Carmelo J. Rizzo, and Michael P. Stone*

Department of Chemistry, Center in Molecular Toxicology, Vanderbilt Ingram Cancer Center, and Center for Structural Biology, Vanderbilt University, Nashville, Tennessee 37235, United States

S *Supporting Information*

ABSTRACT: Michael addition of *trans*-4-hydroxynonenal (HNE) to deoxyguanosine yields diastereomeric 1,N^2-dG adducts in DNA. When placed opposite dC in the 5′-CpG-3′ sequence, the (6S,8R,11S) diastereomer forms a N^2-dG:N^2-dG interstrand cross-link [Wang, H.; Kozekov, I. D.; Harris, T. M.; Rizzo, C. J. *J. Am. Chem. Soc.* **2003**, *125*, 5687−5700]. We refined its structure in 5′-d($G^1C^2T^3A^4G^5C^6\underline{X}^7A^8G^9T^{10}C^{11}C^{12}$)-3′·5′-d($G^{13}G^{14}A^{15}C^{16}T^{17}C^{18}\underline{Y}^{19}C^{20}T^{21}A^{22}G^{23}C^{24}$)-3′ [$X^7$ is the dG adjacent to the C6 carbon of the cross-link or the α-carbon of the (6S,8R,11S) 1,N^2-dG adduct, and Y^{19} is the dG adjacent to the C8 carbon of the cross-link or the γ-carbon of the HNE-derived (6S,8R,11S) 1,N^2-dG adduct; the cross-link is in the 5′-CpG-3′ sequence]. Introduction of ^{13}C at the C8 carbon of the cross-link revealed one ^{13}C8→H8 correlation, indicating that the cross-link existed predominantly as a carbinolamine linkage. The H8 proton exhibited NOEs to Y^{19} H1′, C^{20} H1′, and C^{20} H4′, orienting it toward the complementary strand, consistent with the (6S,8R,11S) configuration. An NOE was also observed between the HNE H11 proton and Y^{19} H1′, orienting the former toward the complementary strand. Imine and pyrimidopurinone linkages were excluded by observation of the Y^{19} N^2H and X^7 N1H protons, respectively. A strong H8→H11 NOE and no $^3J(^{13}C→H)$ coupling for the ^{13}C8−O−C11−H11 eliminated the tetrahydrofuran species derived from the (6S,8R,11S) 1,N^2-dG adduct. The (6S,8R,11S) carbinolamine linkage and the HNE side chain were located in the minor groove. The X^7 N^2 and Y^{19} N^2 atoms were in the gauche conformation with respect to the linkage, maintaining Watson−Crick hydrogen bonds at the cross-linked base pairs. A solvated molecular dynamics simulation indicated that the anti conformation of the hydroxyl group with respect to C6 of the tether minimized steric interaction and predicted hydrogen bonds involving O8H with C^{20} O^2 of the 5′-neighbor base pair $G^5·C^{20}$ and O11H with C^{18} O^2 of $X^7·C^{18}$. These may, in part, explain the stability of this cross-link and the stereochemical preference for the (6S,8R,11S) configuration.
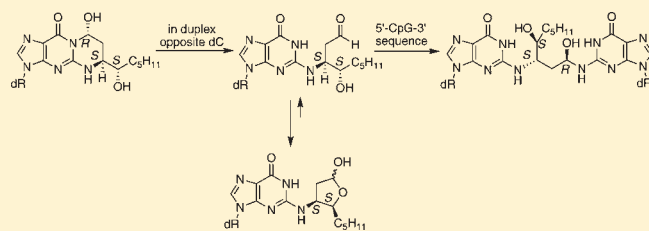
■ INTRODUCTION

trans-4-Hydroxynonenal (HNE) is produced from the metabolism of membrane lipids.[1] It is also the major peroxidation product of ω-6 polyunsaturated fatty acids in vivo.[2,3] Several routes for the formation of HNE from ω-6 polyunsaturated fatty acids have been described.[4−6] HNE exhibits a range of biological effects, from alteration in gene expression and cell signaling to cell proliferation and apoptosis.[7−13] HNE is implicated in the etiologies of a number of diseases associated with oxidative stress, including Alzheimer's disease,[14] Parkinson's disease,[15] arteriosclerosis,[16] and hepatic ischemia reperfusion injury.[17]

HNE induces the SOS response in *Escherichia coli*, suggesting that it is also genotoxic.[18] Chromosomal aberrations have been observed upon exposures to HNE in mammalian, including human, cells.[19−23] In mammalian cells, the genotoxicity of HNE depends upon glutathione levels, which modulate levels of HNE-DNA adducts.[24−26] Michael addition of the N^2-amino group of 2′-deoxyguanosine to HNE gives four diastereomeric 1,N^2-dG adducts 1−4,[27−29] which have been detected in cells.[30−36] Alternatively, oxidation of HNE to 2,3-epoxy-4-hydroxynonanal, and further reaction with nucleobases, affords etheno adducts.[37−41]

Wang et al.[42,43] synthesized the four stereoisomers of the 1,N^2-dG adduct (1−4, Chart 1) and incorporated them into 5′-d(GCTAGC$\underline{Z}$AGTCC)-3′·5′-d(GGACTCGCTAGC)-3′, in which $\underline{Z}$ denotes the HNE-dG adduct. Of the four diastereomeric adducts, only (6S,8R,11S) diastereomer 1 forms interstrand cross-links in the 5′-CpG-3′ sequence. At equilibrium, cross-linking by diastereomer 1 reached >85%.[43] However, it required several months to attain equilibrium at 37 °C.[43] The discovery that when placed into DNA diastereomeric HNE-dG adducts 1 and 3 rearrange to the cyclic hemiacetals provided a rationale for the slow rate of cross-link formation.[44] The hemiacetal effectively masks the reactive aldehyde necessary for cross-link formation.

The major cyclic hemiacetal rearrangement products from HNE-dG adducts 1 and 3 were subsequently examined as to structure in this duplex.[45] Both oriented in the minor groove of DNA. However, the cyclic hemiacetal rearranged from adduct 1 oriented in the 5′-direction, while the cyclic hemiacetal rearranged from adduct 3 oriented in the 3′-direction.[45,46] Molecular mechanics calculations predicted that the N^2-dG aldehyde having

$6R$ configuration oriented in the $3'$-direction, while the N^2-dG aldehyde having $6S$ configuration oriented in the $5'$-direction.[45,46] These differences suggested a kinetic basis to explain, in part, the relative abilities of the $(6S,8R,11S)$ and $(6R,8S,11R)$ diastereomeric adducts **1** and **3** to form cross-links in the $5'$-CpG-$3'$ sequence (Schemes 1 and 2).[43]

In the present work, the structure of this cross-link has been refined in $5'$-d(G^{1}C^{2}T^{3}A^{4}G^{5}C^{6}X^{7}A^{8}G^{9}T^{10}C^{11}C^{12})-$3'$·$5'$-d-(G^{13}G^{14}A^{15}C^{16}T^{17}C^{18}Y^{19}C^{20}T^{21}A^{22}G^{23}C^{24})-$3'$ [X^7 is the dG adjacent to the C6 carbon of the cross-link (the α-carbon of the HNE-derived $(6S,8R,11S)$ 1,N^2-dG adduct **1**), and Y^{19} is the dG

adjacent to the C8 carbon of the cross-link (the γ-carbon of the HNE-derived $(6S,8R,11S)$ 1,N^2-dG adduct **1**); the cross-link is in the $5'$-CpG-$3'$ sequence]. ^{13}C HSQC NMR reveals one ^{13}C8→H8 correlation, indicating that the cross-link exists predominantly as a single species, identified as a $(6S,8R,11S)$ carbinolamine linkage **8**. NOE data indicate that the $(6S,8R,11S)$ carbinolamine linkage **8** and the HNE moiety are oriented in the minor groove. The X^7 N^2 and Y^{19} N^2 atoms are in the gauche-conformation with respect to the linkage, maintaining Watson–Crick hydrogen bonds at the cross-linked base pairs. Solvated molecular dynamics simulations indicate that the anti conformation of the hydroxyl group with respect to C6 of the tether minimizes steric interaction and predict a hydrogen bond between the hydroxyl group and C^{20} O^2 of the $5'$-neighbor base pair G^5·C^{20}. As well, the C11 hydroxyl predominantly formed a hydrogen bond with C^{18} O^2. These hydrogen bonds may, in part, explain the stability of this cross-link and the preference for the $(6S,8R,11S)$ configuration **8**.
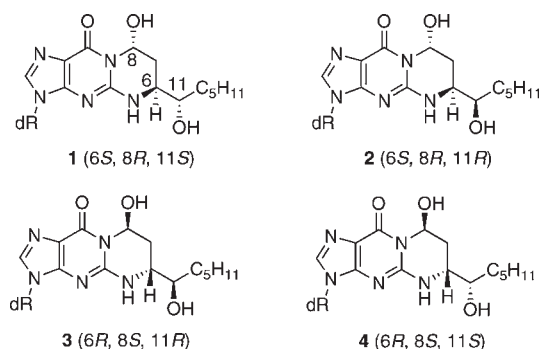
■ RESULTS
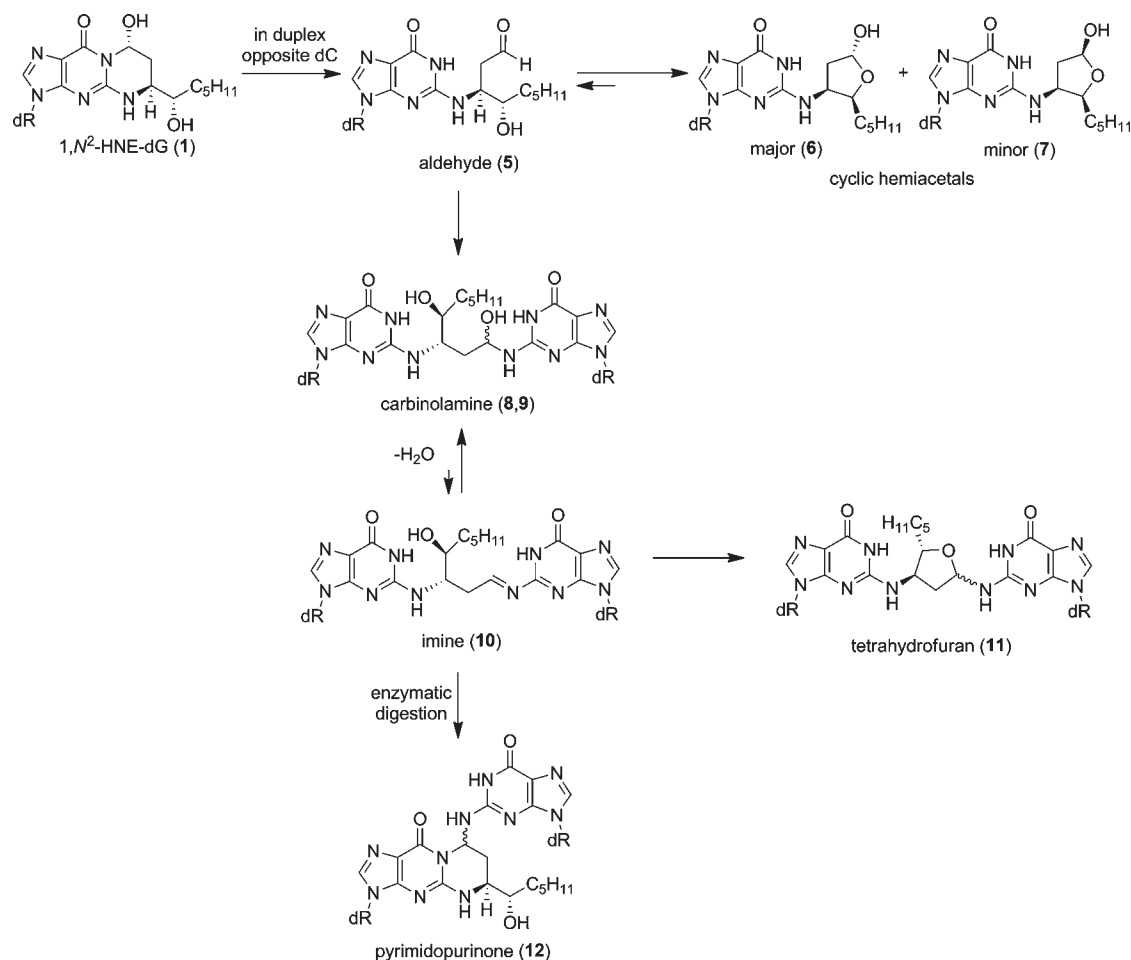
Formation of the Cross-link. The oligodeoxynucleotide $5'$-d(GCTAGCZAGTCC)-$3'$ [Z = $(6S,8R,11S)$ HNE adduct **1**] was annealed with the complementary strand $5'$-d(GGACT-CGCTAGC)-$3'$ at pH 7.0. The duplex was maintained at 37 °C for 3 months at pH 7.3. This afforded the N^2-dG:N^2-dG cross-link, as reported.[43] The presence of the cross-link was confirmed

Chart 1

1 (6S, 8R, 11S)

2 (6S, 8R, 11R)

3 (6R, 8S, 11R)

4 (6R, 8S, 11S)

Scheme 1. Formation of the N^2-dG:N^2-dG Cross-link by the Oligodeoxynucleotide Duplex Containing the HNE Adduct 1 in the $5'$-CpG-$3'$ Sequence

1,N^2-HNE-dG (**1**)

aldehyde (**5**)

major (**6**)   minor (**7**)

cyclic hemiacetals

carbinolamine (**8,9**)

-H_2O

imine (**10**)

tetrahydrofuran (**11**)

enzymatic digestion

pyrimidopurinone (**12**)

Scheme 2. (A) Numbering Scheme of the Duplex Containing (6S,8R,11S) 1,N^2-dG Adduct 1;[a,b] and (B) Numbering Scheme of the (6S,8R,11S) Carbinolamine Cross-link 8[a,c,d]
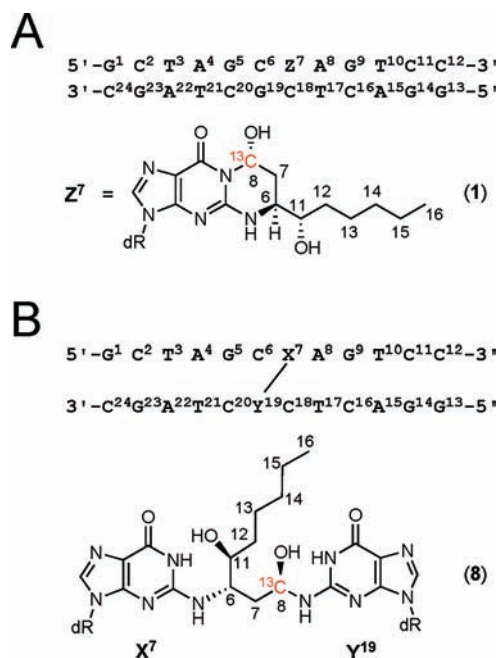
[a] The ^{13}C labeled carbon is in red. [b] Z^7 represents the HNE adduct **1**. [c] X^7 and Y^{19} represent the N^2-cross-linked deoxyguanosines; the atoms are numbered as for deoxyguanosine. [d] The atom numbers of the HNE linkage are consistent with those in the HNE adduct **1**.

by reverse-phase HPLC analysis (Figure S1 in the Supporting Information). The cross-link was also characterized by MALDI-TOF mass spectrometry, which showed the cross-link at m/z of 7428.2 [calculated for imine cross-link **10** (M − 1): 7429.0] (Figure S2 in the Supporting Information). The intensities of the cytosine H5−H6 NMR scalar couplings were used to evaluate the extent of the DNA cross-linking reaction (Figure S3 in the Supporting Information). HPLC analysis suggested the duplex was >75% cross-linked.

NMR Resonance Assignments. The cross-linked sample was used for NMR experiments without further purification. The spectra were of high quality and suitable for structural analysis. The assignments of the nonexchangeable protons of the nucleotides were accomplished using standard protocols.[47,48] For the 5′-d($G^1C^2T^3A^4G^5C^6\underline{X}^7A^8G^9T^{10}C^{11}C^{12}$)-3′ strand, complete NOE connectivity was observed between the aromatic and anomeric protons (Figure S4 in the Supporting Information). A small cross peak was assigned to the C^6 H1′→X^7 H8 correlation. Complete NOE connectivity was also observed for the 5′-d($G^{13}G^{14}A^{15}$-$C^{16}T^{17}C^{18}Y^{19}C^{20}T^{21}A^{22}G^{23}C^{24}$)-3′ strand. With the exceptions of several of the H4′ protons, and the stereotopic assignments of the H5′ and H5″ sugar protons, all other assignments were made unequivocally. In general, canonical B-DNA distances between the H4′, H5′, and H5″ protons were used to tentatively assign the H5′ and H5″ deoxyribose protons. The chemical shifts of the nonexchangeable DNA protons are collected in Table S1 of the Supporting Information. As compared to the corresponding unmodified duplex, remarkable changes in chemical shifts were observed for protons located in the cross-linked region, suggesting perturbation of the cross-linked and the flanking base pairs (Figure S5 in the Supporting Information).
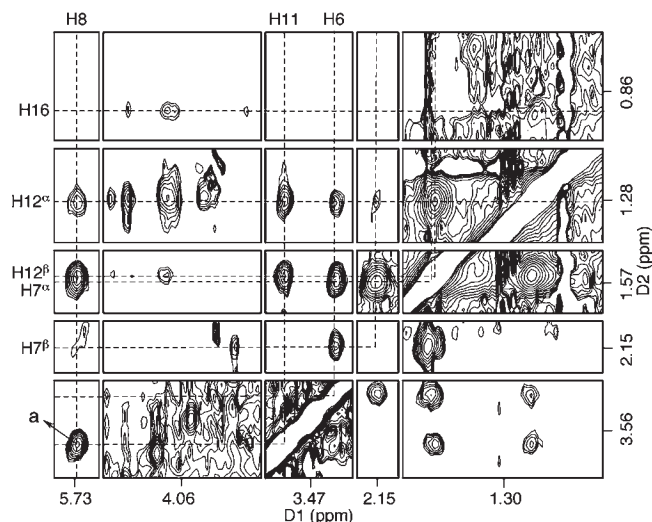

Figure 1. Expansions of the ^{1}H−^{1}H NOESY spectrum obtained at a mixing time of 60 ms of the cross-link showing the assignments of some HNE protons. The strong H8→H11 NOE (peak a) implies the cross-link exists as carbinolamine **8**.

The imino proton resonances of Watson−Crick base paired guanines and thymines were also assigned following standard protocols.[49] The imino proton resonances were observed for all guanines and thymines, and a complete NOE connectivity was obtained, with the exceptions of the terminal guanines G^1 and G^{13}, the resonances of which were broadened by solvent exchange (Figure S6 in the Supporting Information). The X^7 N1H→C^{18} N^4H(s) and Y^{19} N1H→C^6 N^4H(s) NOEs were observed, indicating the presence of the $C^6 \cdot Y^{19}$ and $X^7 \cdot C^{18}$ pairs at the cross-linked site. Strong X^7 N1H→X^7 N^2H and Y^{19} N1H→Y^{19} N^2H NOEs were observed, also consistent with Watson−Crick base pairing at the cross-linked site. The X^7 N1H→A^8 H2 NOE was also observed, consistent with the intrahelical stacking of the modified nucleotide X^7.

The assignments of HNE protons were made by a combination of ^{1}H−^{1}H NOESY (60 ms) (Figure 1), ^{1}H−^{1}H DQF-COSY, and ^{1}H−^{1}H TOCSY experiments. The HNE H6 and H8 protons were assigned by inspection of the H6→X^7 N^2H and H8→Y^{19} N^2H NOEs. Both of these protons exhibited scalar and dipolar coupling with the geminal HNE H7 protons. H6 also exhibited scalar and dipolar coupling with H11. H11 exhibited scalar and dipolar coupling with the geminal H12 protons. The protons in the HNE side-chain were partially assigned sequentially based on the scalar and dipolar couplings from H12→H13→H14→H15→H16. The geminal H7 and H11 protons exhibited strong scalar and dipolar couplings. The absolute configurations of the geminal H7 protons were determined by their NOEs with H8. H7$_\beta$, which was in the trans configuration with respect to H8, showed a smaller dipolar coupling with H8 than did H7$_\alpha$. The stereotopic assignments of the geminal H12 protons could not be unequivocally determined. The intensities of the H11→H12$_\alpha$ and H11→H12$_\beta$ NOEs appeared equal, indicating H11 was in the gauche conformation with respect to both protons. A number of NOEs between these HNE protons and the DNA protons X^7 N1H, X^7 N^2H, Y^{19} N1H, and Y^{19} N^2H were observed. The chemical shifts of the HNE protons and the NOEs used for the rMD calculations are listed in Table 1.

Table 1. Chemical Shifts of the HNE Protons and NOEs Used for rMD Calculations. [a]

proton	δ (ppm)	NOE
H6	3.47	H7$_\alpha$ (s); H7$_\beta$ (s); H8 (m); H12$_\alpha$ (s); H12$_\beta$ (s); X[7] H1′ (w); A[8] H1′ (w); A[8] H2 (w); A[8] H4′ (w)
H7$_\alpha$	1.57	H8 (s); A[8] H1′ (w)
H7$_\beta$	2.15	H8 (s); H11 (w); H12$_\alpha$ (m); A[8] H1′ (w)
H8	5.74	H11 (s); H12$_\alpha$ (s); H12$_\beta$ (s); Y[19] H1′ (w); C[20] H1′ (m); C[20] H4′ (m)
H11	3.61	H12$_\alpha$ (s); H12$_\beta$ (s)
H12$_\alpha$	1.29	A[8] H4′ (m); G[9] H4′ (m)
H12$_\beta$	1.56	H16 (m); A[8] H4′ (m); G[9] H4′ (w); Y[19] H4′ (m); C[20] H4′ (m); C[20] H5′ (m)
H13	1.21	X[7] H4′ (m); C[20] H4′ (m)
H14	1.34	H16 (m); X[7] H4′ (m); Y[19] H4′ (m); C[20] H4′ (m); C[20] H5′ (m)
H15	1.28	H16 (s); X[7] H4′ (m); G[9] H4′ (m)
H16	0.85	X[7] H4′ (m); G[9] H4′ (w); Y[19] H4′ (w); C[20] H4′ (m); C[20] H5′ (m)

[a] Letters in brackets indicate peak intensity: s, strong; m, medium; w, weak.
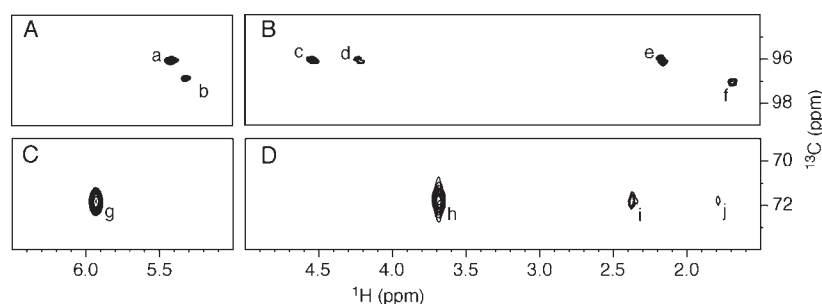
Figure 2. $^1H-^{13}C$ HSQC and $^1H-^{13}C$ HMBC spectra of the ^{13}C-labeled duplex. (A) $^1H-^{13}C$ HSQC before cross-linking; peaks are designated (a) H8→C8 of cyclic hemiacetal **6** and (b) H8→C8 of cyclic hemiacetal **7**. (B) $^1H-^{13}C$ HMBC before cross-linking; peaks are designated (c) H6→C8, (d) H11→C8, (e) H7→C8 of cyclic hemiacetal **6**, (f) H7→C8 of cyclic hemiacetal **7**. (C) $^1H-^{13}C$ HSQC after cross-linking; peak is designated (g) H8→C8 of the cross-link **8**. (D) $^1H-^{13}C$ HMBC after cross-linking; peaks are designated (h) H6→C8, (i) H7$_\beta$→C8, (j) H7$_\alpha$→C8 of cross-link **8**.

Identification of the Cross-link. The introduction of ^{13}C at the γ carbon of HNE adduct **1** enabled the chemistry of cross-linking to be monitored, in situ. Figure 2 displays the $^1H-^{13}C$ HSQC and $^1H-^{13}C$ HMBC spectra of the sample before and after cross-linking. The $^1H-^{13}C$ HSQC spectrum of the ^{13}C-labeled sample exhibited a strong C8→H8 correlation (Figure 2), indicating that only one cross-link species was produced. Of the four potential species for the cross-link (Scheme 1), imine **10** and pyrimidopurinone **12** were excluded as the observed cross-links by the observation of Y[19] N^2H and X[7] N1H protons, respectively. The cyclic hemiacetal **6** derived from HNE adduct **1** contains a THF unit and exhibited a $^3J(^{13}C$→H) coupling for the C8—O—C11—H11. The cross-link did not exhibit this correlation. The cross-link exhibited NOE correlations for H8 with Y[19] H1′, C[20] H1′, and C[20] H4′ (Figure 3), suggesting H8 oriented toward the complementary strand. The cross-link also exhibited the H11→Y[19] H1′ NOE, suggesting that H11 oriented in the same direction toward the complementary strand. A strong H8→H11 NOE was observed (Figure 1). Molecular modeling indicated that the THF cross-link **11** placed the H8 and H11 in the trans configuration, with H11 oriented toward the 5′-d(G[1]C[2]T[3]A[4]G[5]-C[6]X[7]A[8]G[9]T[10]C[11]C[12])-3′ strand, such that a strong H8→H11 NOE correlation was not possible (Figure S7 in the Supporting Information). In contrast, the carbinolamine cross-link could place both H8 and H11 toward the complementary strand with a distance of less than 3 Å. Therefore, the cross-link derived from the (6S,8R,11S) HNE-dG adduct **1** existed as carbinolamine **8** or **9**.
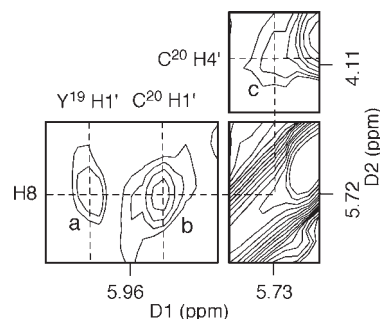

Figure 3. Expansions of the $^1H-^1H$ NOESY spectrum obtained at a mixing time of 250 ms of the cross-link. NOEs used to determine the configuration of C8 are assigned as (a) Y[19] H1′→H8; (b) C[20] H1′→H8; and (c) H8→C[20] H4′.

Stereochemistry of the Cross-link. Formation of a carbinolamine cross-link from the N^2-dG aldehydic adduct **5** creates a chiral center at C8 (Chart 2). The orientation of H8 toward the complementary strand indicated the R-configuration at the C8 position. Thus, the N^2-dG:N^2-dG cross-link derived from the (6S,8R,11S) HNE-dG adduct **1** existed as (6S,8R,11S) carbinolamine **8**.

Stability of the Cross-link. The resonances of thymine N3H and guanine N1H imino protons at different temperatures are shown in Figure 4. The melting temperature T_m of the cross-link was >90 °C in 1 M NaCl buffer, confirming previous measurements.[43]

Chart 2. Structures of the (6S,8R,11S) and (6S,8S,11S) Carbinolamine Cross-links

8 (6S,8R,11S)   **9 (6S,8S,11S)**
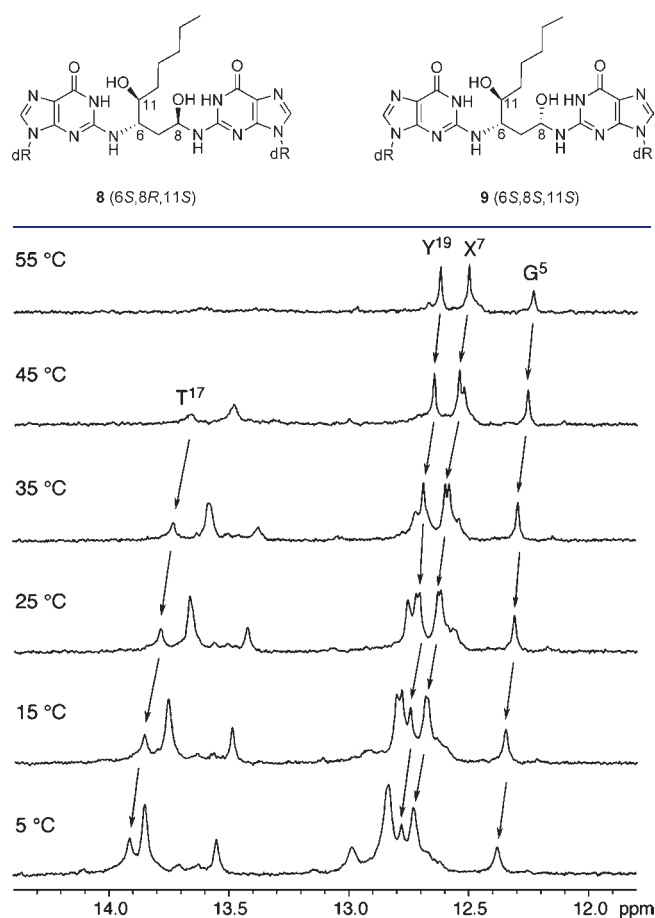
Figure 4. ^{1}H NMR of the imino proton region of the cross-linked duplex as a function of temperature.

Consistent with the high melting temperature, the X^7 and Y^{19} imino resonances remained sharp at 55 °C. For the 5′-neighbor base pair $G^5 \cdot C^{20}$, the G^5 imino resonance also remained sharp at 55 °C, albeit more broadened than the X^7 and Y^{19} imino resonances. In contrast, other guanine N1H protons were not observed at 55 °C. At the 3′-neighbor $A^8 \cdot T^{17}$ base pair, the T^{17} imino resonance was broadened at 45 °C and not observed at 55 °C. This was comparable with the other thymine N3H protons. This indicated that the cross-linked and 5′-neighbor $G^5 \cdot C^{20}$ base pairs were stabilized by the cross-linking, whereas the 3′-neighbor $A^8 \cdot T^{17}$ base pair was not affected.

Structural Refinement. The structural refinement involved 372 distance restraints, including 203 intranucleotide and 169 internucleotide restraints, which were obtained from the intensities of NOE cross peaks. In addition, 52 empirical distance restraints defining Watson−Crick base pairing were used to refine the structure of the duplex; their use was predicated upon inspection of the NMR data, which indicated that Watson−Crick base pairing was intact throughout the duplex. Finally, an additional 180 empirical backbone torsion angle restraints were also used for structure refinement; these were based upon inspection of the NMR data, which suggested that the adducted duplex maintained a B-family architecture. The NOE restraints used for the structural refinement are listed in Table S2 in the Supporting Information.

Table 2. rMD Restraints and Statistical Analysis of rMD Structures of the Cross-link

total restraints used for rMD calculation	604
experimental NOE distance restraints[a]	372
intraresidue NOE restraints	203
inter-residue NOE restraints	169
NOE restraints for HNE linkage	46
base pairing distance restraints	52
backbone torsion angle restraints	100
sugar puckering restraints	80
structural analysis	
NMR R-factor (R_1^x) $(\times 10^{-2})$[b]	8.4
intraresidue	7.6
inter-residue	9.7
rmsd deviation of refined structures (Å)	0.48

[a] HNE unit was considered to be a single residue attached to guanines X^7 and Y^{19} in the rMD calculations and the statistical analyses. [b] Mixing time used to calculate R_1^x was 250 ms. $R_1^x = \Sigma |(a_0)_i^{1/6} - (a_c)_i^{1/6}| / |(a_0)_i^{1/6}|$, where (a_0) and (a_c) are the intensities of observed (nonzero) and calculated NOE cross peaks, respectively.

The randomly seeded rMD calculations were performed starting with initial structures, which were created either with A- or with B-form conformations.[50] The force field parameters used for the cross-link are provided in Figure S8 of the Supporting Information. Pairwise rmsd analysis of emergent structures indicated that the calculations converged, irrespective of starting structure (Table 2). The accuracies of the emergent structures were evaluated by comparison of theoretical NOE intensities calculated by complete relaxation analysis[51] of the refined structure, to the experimental NOE intensities, to yield sixth root residuals (R_1^x).[52,53] This residual was less than 0.1 for the modified duplex (Table 2), and the inter- and intranucleotide residuals for individual nucleotides were less than 0.15, indicating that the refined structures provided an accurate depiction of the NOE data. The residue-by-residue R_1^x values are shown in Figure S9 of the Supporting Information.

Structure of the Cross-link. The refined structure of the (6S,8R,11S) carbinolamine cross-link maintained B-family DNA conformation (Figure S10 of the Supporting Information). All nucleotides maintained the anti conformation about the glycosyl torsion angles. The deoxyribose pseudorotations were consistently either $C_{1'}$-exo or $C_{2'}$-endo. The helicoidal analysis of the backbone torsion angles of the refined structure is shown in Figure S11 of the Supporting Information. Perturbations of ζ angle $(C3'−O3'−P−O5')$ were observed at cross-linked bases X^7 and Y^{19}. This is consistent with the observation of two downfield shifted ^{31}P resonances (Figure S12 of the Supporting Information). An expanded view from the minor groove at the cross-linked region is displayed in Figure 5. A perturbation was observed for the cross-linked and the 3′-neighbor $A^8 \cdot T^{17}$ base pairs, whereas no perturbation was observed for the 5′-neighbor $G^5 \cdot C^{20}$ base pair. Figure 6 shows the base pairing of the cross-linked and flanking base pairs.

The 3-carbon linkage of the cross-link was folded in the minor groove. Figure 7 demonstrates the conformation of the linkage and the Newman projections viewed along the C6−C7, C7−C8, and C6−C11 bonds. Both X^7 N^2 and Y^{19} N^2 were in the gauche-conformation with respect to C6 and C8, respectively, which facilitated the Watson−Crick hydrogen bonding of the $C^6 \cdot Y^{19}$
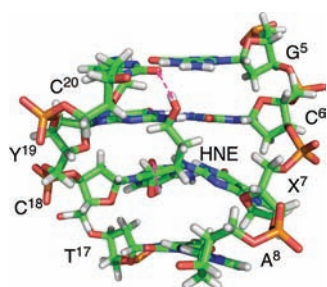
Figure 5. Expanded view of the average structure of 10 refined structures of the cross-link from the minor groove. The aliphatic chain of HNE is not shown. The predicted hydrogen bonds involving the HNE hydroxyl groups are indicated with pink arrows.
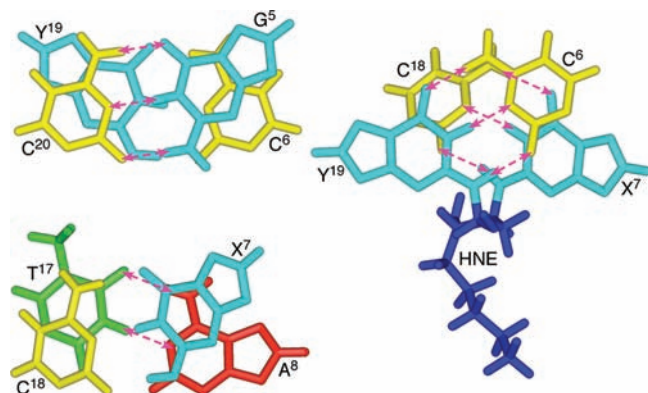

Figure 6. Base pairing and base stacking of the cross-link at the cross-linked region. The predicted hydrogen bonds are indicated by the pink arrows.
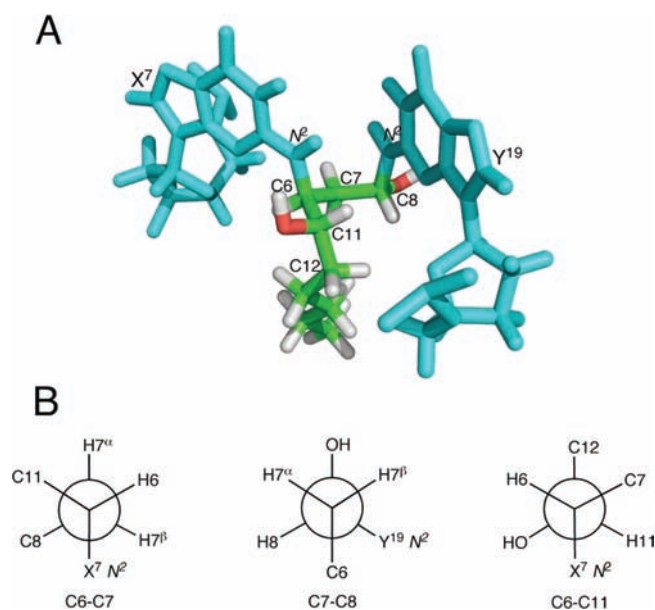

Figure 7. (A) Conformation of the HNE linkage of the cross-link. (B) Newman projections viewed along the C6−C7, C7−C8, and C6−C11 bonds.

and $X^7 \cdot C^{18}$ base pairs. The large substituent groups were in either the trans- or gauche-conformations, minimizing steric

Table 3. Occupancies of Potential Hydrogen-Bonding Interactions Involving the HNE Hydroxyl Groups in Molecular Dynamics Simulations

donors	hydrogen-bond receptors[a]					
	$C^6 O^2$	$A^8 N3$	$C^{18} O^2$	$C^{20} O^2$	$C^{20} O4'$	solvent
O8H	1.2	0.0	0.0	98.0	0.1	0.1
O11H	0.0	0.6	99.4	0.0	0.0	0.0

[a] Criteria for hydrogen-bond formation: distance < 3.5 Å and angle > 120°.

interactions. Two hydrogen bonds were predicted for the hydroxyl groups of the HNE linkage (Figure 5). The O8H was predicted to hydrogen bond with $C^{20} O^2$, and O11H was predicted to hydrogen bond with $C^{18} O^2$.

Molecular Dynamics Simulations. Molecular dynamics simulations in explicit solvent were carried out to assess the potential for hydrogen-bond formation involving the hydroxyl groups of the HNE linkage. A fully solvated molecular dynamics simulation of 5 ns was carried out starting from the refined structure of the cross-link (Figure S13 of the Supporting Information). The all-atom mass-weighted root-mean-square deviations (RMSDs) referenced to the starting structures were used to categorize the conformation of the trajectories. Two major conformers were observed for the cross-link during the molecular dynamics simulations.

The MD trajectories were used to analyze the potential hydrogen bonding of the carbinol hydroxyl group of the tether. Table 3 lists the occupancies of the hydroxyl groups by the potential hydrogen-bond acceptors in the MD trajectories. As predicted by the refined structures, irrespective of which conformation the cross-link adopted, the O8H predominantly formed a hydrogen bond with $C^{20} O^2$, and the O11H predominantly formed a hydrogen bond with $C^{18} O^2$. The occupancies involving hydrogen bonds with other receptors were negligible. Water molecules were not involved in the hydrogen-bond formation with either of the hydroxyl groups throughout the simulations.

■ DISCUSSION

DNA interstrand cross-links represent one of the most serious types of DNA damage, because fundamental biological processes, such as replication and transcription, require transitory separation of the DNA strands. Findings that HNE, the major in vivo peroxidation product of ω-6 polyunsaturated fatty acids,[1−3] induces DNA cross-linking[46] are consistent with cytotoxicity induced by HNE.[54] Several signaling pathways, including heat shock response activation, NF-κB inactivation, JNK activation, and *p53* target gene expression links to cell apoptosis, are significantly influenced by HNE.[12] DNA damage may also activate the *p53* damage response.[55] Additional interest in the cross-linking abilities of the stereoisomers of HNE-derived 1,N^2-dG adducts **1**−**4** arose from studies of the corresponding 1,N^2-dG adducts of acrolein and crotonaldehyde, which formed reversible cross-links in this 5′-CpG-3′ sequence, comprised of carbinolamine-type linkages in equilibrium with trace amounts of imines.[56,57]

Chemistry of HNE-Induced DNA Cross-linking. Kozekov et al.[58,59] trapped a trimethylene cross-link upon insertion of the acrolein-derived γ-OH-PdG adduct into this oligodeoxynucleotide duplex at the 5′-CpG-3′ sequence by NaCNBH$_3$ treatment. This implied the presence of the imine linkage, in equilibrium with the carbinolamine linkage. Enzymatic digestion of the cross-linked DNA afforded a cross-linked pyrimidopurinone,[58]

although it was not clear if the latter was also in equilibrium with the carbinolamine and imine or if it was formed after the digestion. In contrast, ^{1}H$-^{15}$N HSQC NMR detected the presence of the carbinolamine linkage,[60] as did ^{13}C isotope-edited approaches.[61,62] Isotope-edited NMR has also been applied to characterizing the chemistry of crotonaldehyde-mediated DNA cross-linking.[63] Because the carbinolamine, imine, and potentially the pyrimido-purinone linkages exist in equilibrium (Scheme 1), monitoring the composition of the mixtures in situ is of considerable interest. All three cross-linked species may contribute to the biological processing of enals. The present studies apply isotope-edited NMR to the chemistry of HNE-mediated DNA cross-linking in the 5′-CpG-3′ sequence. The HNE adduct was synthesized with a specific ^{13}C-label at the aldehyde carbon, which is position-8 of the pyrimidopurinone structure **12**. The strong ^{13}C8→H8 corre-lation observed in the ^{1}H$-^{13}$C HSQC spectrum (Figure 2) indicated that at equilibrium, one cross-linked species predomi-nated. The identification of the carbinolamine linkage was supported by observation of NOE correlations for HNE H8 with Y^{19} H1′, C^{20} H1′, and C^{20} H4′ (Figure 3), suggesting H8 oriented toward the complementary strand. The cross-link also exhibited the H11→Y^{19} H1′ NOE, suggesting that H11 oriented in the same direction toward the complementary strand. A strong HNE H8→HNE H11 NOE was observed (Figure 1). The carbinolamine places both HNE H8 and HNE H11 toward the complementary strand with a distance of less than 3 Å. The carbinolamine cross-link **8** is expected to epimerize at the C8 carbon. The NOE data for the H8 proton indicate that the C8 carbon prefers the *R*-configuration.

The diastereomeric 1,N^2-dG adducts **1** and **3** rearrange to the N^2-dG cyclic hemiacetals when placed into DNA.[44] It had been hypothesized that the significant levels observed for formation of HNE-induced cross-links in the 5′-CpG-3′ DNA sequence could be due to the presence of the corresponding tetrahydrofuran **11**, which might stabilize the cross-link.[43] This does not appear to be the case. The cyclic hemiacetal **6** derived from HNE adduct **1** exhibits a ^3J(^{13}C→H) coupling for the C8–O–C11–H11. The carbinolamine cross-link **8** did not exhibit this correlation. Rather, the strong H8→H11 NOE and failure to observe ^3J (C8–O–C11–H11) coupling suggested that the cross-link existed as carbinolamine **8**. Moreover, molecular modeling suggested that the cyclic hemiacetal containing cross-link **11** placed the HNE H8 and H11 in the trans configuration, with H11 oriented toward the 5′-d(G^{1}C^{2}T^{3}A^{4}G^{5}C^{6}X^{7}A^{8}G^{9}T^{10}C^{11}C^{12})-3′ strand, such that a strong H8→H11 NOE correlation should not have been observed. Additionally, pyrimidopurinone linkage **12** has been isolated by HPLC and characterized by mass spectrometry when the cross-link is enzymatically digested.[43] However, the presence of significant equilibrium levels of either imine linkage **10** or pyrimidopurinone linkage **12** (Scheme 1) is excluded by the observation of Y^{19} N^2H and X^7 N1H protons, respectively.

Conformation of the Cross-link. The 3-carbon tether is too short to span the guanines in the N^2-dG: N^2-dG cross-link, forcing the cross-linked C^6·Y^{19} and X^7·C^{18} base pairs to tilt toward each other (Figure 5). This has been observed for other N^2-dG:N^2-dG cross-links bridged by three-carbon tethers.[62,64] The base stacking of C^6·Y^{19} with the 5′-neighbor G^5·C^{20} is not perturbed, whereas the base stacking of X^7·C^{18} with the 3′-neighbor A^8·T^{17} is perturbed (Figure 6). Despite the fact that A^8·T^{17} is the 3′-neighbor of the cross-linked base pairs, its stability is comparable to that of other A·T base pairs (Figure 4). The gauche conformations of the HNE C6 and C8 carbons with

respect to the cross-linked guanine N^2 amines facilitate Watson−-Crick hydrogen bonding of the cross-linked C^6·Y^{19} and X^7·C^{18} base pairs (Figure 7). This has also been observed with other N^2-dG:N^2-dG cross-links.[62,64−66] The HNE linkage adopts a low energy conformation by placing all of the substituent groups in either trans- or gauche-orientations (Figure 7). The small cross peaks assigned to the C^6 H1′→X^7 H8 and C^{18} H1′→Y^{19} H8 correlations were observed for other cross-links in the 5′-CpG-3′ sequence that were bridged by the trimethylene,[67,68] α-methyltrimethyl,[64] or the carbinolamine derived from the acrolein 1,N^2-dG adduct.[62]

The stabilization of (6*S*,8*R*,11*S*) carbinolamine cross-link[43] **8** appears to be mediated by hydrogen-bonding interactions. The solvated equilibrium molecular dynamics simulations predict hydrogen bonds between O8H and C^{20} O^2, and between O11H and C^{18} O^2 (Figure 5). In contrast, the (6*S*,8*S*,11*S*) carbinola-mine cross-link, which is not observed, would have placed the O8H in a gauche-configuration with respect to C6, and the O8H→C^{20} O^2 hydrogen bond would not be possible. Thus, it seems plausible that the O8H→C^{20} O^2 hydrogen bond stabilizes the carbinolamine linkage and accounts for the stereoselectivity of cross-linking, favoring the (6*S*,8*R*,11*S*) cross-link **8**. As well, formation of a O11H→C^{18} O^2 hydrogen bond further stabilizes the (6*S*,8*R*,11*S*) carbinolamine cross-link. These hydrogen bonds may also explain why carbinolamine cross-link **8** does not exist as the tetrahydrofuran **11**, as the removal of two these hydroxyl groups and their hydrogen-bonding capabilities with the DNA would disfavor the latter.

Comparison with Acrolein- and Crotonaldehyde-Derived Cross-links. The acrolein-derived 1,N^2-dG adduct also induces a N^2-dG:N^2-dG cross-link in the 5′-CpG-3′ sequence,[58,59] as do the two diastereomeric crotonaldehyde-derived 1,N^2-dG adducts.[59,63] These cross-links exist predominantly as carbinolamine linkages for both acrolein and crotonaldehyde adducts. The acrolein cross-link favors the *R*-carbinolamine linkage, but the *S*-carbino-lamine linkage is detectable by NMR.[62] The structure of the cross-link indicates that base stacking of the cross-linked base pair with the 3′-flanking base pair is not affected by the cross-linking. This is consistent with the trimethylene N^2-dG:N^2-dG cross-link, which has been used as a model.[62] Similarly, a hydrogen bond involving the carbinol hydroxyl group with the 5′-flanking cytosine O^2 is predicted to stabilize the cross-link and account for the stereoselectivity.[62] The *R*-isomer of the crotonaldehyde adduct at the C6 position forms the cross-link more efficiently than does the *S*-isomer.[59] Significantly, the 6*R*-isomer of the crotonaldehyde adduct has the same relative configuration as does the (6*S*,8*R*,11*S*) HNE adduct **1**. The stereoisomeric α-methyltrimethylene cross-links have been used as surrogates for these carbinolamine cross-links.[64] The *S*-CH$_3$ group inter-feres with the 3′-flanking base pair, whereas the *R*-CH$_3$ group does not. As compared to the crotonaldehyde α-CH$_3$ group, the 3′-oriented HNE aliphatic chain has greater influence on the 3′-flanking base pair. Poor base stacking was observed between X^7·C^{18} and A^8·T^{17} base pairs (Figure 6).

Biological Implications. In humans, DNA cross-link repair requires the cooperation of multiple proteins belonging to different biological pathways, including, but not limited to, nucleotide excision repair, homologous recombination, translesion DNA synthesis, double-strand break repair, and the Fanconi anemia pathway.[54,69−73] Current models suggest that cross-link repair is initiated by dual incisions around the cross-link in one of the two affected strands. This "unhooking" depends on the endonucleolytic activity of the XPF/ERCC1 complex, a component of NER. The

result is a gap that may be filled by pairing of the 3′-terminus of the preincised strand with the homologous sequence, followed by DNA synthesis. Alternatively, the complementary strand with the cross-link attached may be used as a template for translesion DNA synthesis. Once the integrity of one DNA strand is restored, the second strand may be repaired by conventional NER. When repair is concomitant with replication, a DNA double-strand break is formed; thus, additional biological processing would be required to tolerate interstrand cross-links.[54,70]

Because enal-mediated cross-links are reversible, prior studies have utilized the fully reduced trimethylene N^2-dG:N^2-dG cross-links as models to address molecular mechanisms of repair. A role for XPF/ERCC1 heterodimer in the processing of a double strand break (DSB) was created when the saturated cross-link encounters the replication fork.[74] It has been proposed that the cross-link repair is initiated by NER followed by trans-lesion DNA synthesis (TLS) and completed through another round of NER in *E. coli*.[75] Liu et al.[76] examined the repair of crotonaldehyde-derived N^2-dG:N^2-dG cross-links following replication of site-specifically modified vectors in *E. coli* and mammalian cells. Their results suggest that the native cross-link partially reverts and are consistent with reports that NER is essential for repair in *E. coli*.[77,78] In XPA cells, the reduced cross-link is removed, suggesting a repair pathway unique to higher eukaryotes that does not require damage recognition by NER.[76] Minko et al.[79] reported that a vector containing a model of the incised product following dual incision around the saturated N^2-dG:N^2-dG trimethylene cross-link is replicated in mammalian cells. Human polymerase κ catalyzes accurate incorporation opposite this cross-link and also elongates the sequence. The reversibility of the HNE derived cross-links, noted by Liu et al.,[35] might reduce their abilities to block DNA processing, in vivo. Cross-link reversion would be anticipated to target removal of the resulting bulky N^2-dG adducts by NER.[80−82]

In light of the observation that the (6S,8R,11S) HNE-derived adduct **1** forms cross-links in 5′-CpG-3′ DNA sequences in vitro,[42,43] it is anticipated that the cross-linking will also occur in vivo. Cross-links were observed at levels of 1−2% that of the uncross-linked adduct when calf thymus DNA was treated with acrolein and HNE,[83] and it will be of interest to search for this reversible HNE-derived cross-link in cellular DNA. Because they occur specifically at 5′-CpG-3′ sequences, and only for (6S,8R,11S) HNE adduct **1**, they are anticipated to be present at low levels in vivo, challenging the limits of detection by mass spectrometry. On the other hand, the genotoxic and cytotoxic consequences arising from low levels of this cross-link may be of considerable significance.

■ SUMMARY

HNE-derived (6R,8S,11R) 1,N^2-dG adduct **1** produces the (6R,8S,11R) carbinolamine cross-link **8** in the 5′-CpG-3′ DNA sequence. The HNE moiety is located in the minor groove. Hydrogen bonds between O8H and C^{20} O^2 and between O11H and C^{18} O^2 are predicted to stabilize cross-link formation. They are also proposed to account for the stereoselectivity and result in the higher yield by HNE adduct as compared to acrolein and crotonaldehyde adducts.

■ EXPERIMENTAL SECTION

Materials. The oligodeoxynucleotide 5′-GGACTCGCTAGC-3′ was synthesized and purified by anion-exchange chromatography by the Midland Certified Reagent Co. (Midland, TX). The oligodeoxynucleotides containing HNE derived (6S,8R,11S) 1,N^2-dG adducts **1** in the dodecamer 5′-d(GCTAGCXAGTCC)-3′, where X represents the HNE adduct, were synthesized, purified, and characterized as reported.[42,43] The purities of the adducted oligodeoxynucleotides were assessed by capillary gel electrophoresis and HPLC. Oligodeoxynucleotides were desalted by chromatography on Sephadex G-25. The synthesis of isotope-labeled oligodeoxynucleotides is described in the Supporting Information.

Preparation of the Cross-link. The oligodeoxynucleotide 5′-d(GCTAGCXAGTCC)-3′ containing HNE adduct **1** was annealed with the complementary strand 5′-d(GGACTCGCTAGC)-3′ in buffer containing 10 mM NaH_2PO_4, 100 mM NaCl, and 50 μM Na_2EDTA (pH 7.0). The solution was heated to 95 °C for 10 min, then slowly cooled to room temperature. The duplex was purified by DNA grade hydroxylapatite chromatography with a gradient from 10 to 200 mM NaH_2PO_4 in 100 mM NaCl, 50 μM Na_2EDTA (pH 7.0), and then desalted using Sephadex G-25. The duplex was then dissolved in 10 mM NaH_2PO_4, 100 mM NaCl, and 50 μM Na_2EDTA (pH 7.0). The pH was adjusted to 7.3. The sample was maintained at 37 °C for 3 months. The cross-linking was monitored by observing the cytosine H5−H6 scalar couplings by NMR. After 3 months, the sample was used for NMR experiments without further purification. HPLC analysis suggested the duplex was >75% cross-linked. The MALDI-TOF mass spectrometry showed the cross-link at m/z of 7428.2 [calculated for imine cross-link **10** (M − 1): 7429.0].

NMR. Samples were at 1.0 mM strand concentration. Samples for observation of nonexchangeable protons were dissolved in 280 μL of buffer containing 10 mM NaH_2PO_4, 100 mM NaCl, and 50 mM Na_2EDTA (pH 7.0). They were exchanged with D_2O and suspended in 280 μL of 99.996% D_2O. The pH was adjusted to 7.3 with dilute DCl or NaOD. Samples for the observation of exchangeable protons were dissolved in 280 μL of 10 mM NaH_2PO_4, 100 mM NaCl, and 50 μM Na_2EDTA, (pH 7.0) containing 9:1 H_2O:D_2O (v/v) and the pH was adjusted to 7.3. ^1H−^{13}C HSQC and ^1H−^{13}C HMBC experiments experiments[76−78] were performed on a Bruker Avance 500 spectrometer. Other NMR experiments were performed on a Bruker Avance 800 spectrometer. The temperature was 25 °C for observation of the nonexchangeable protons and 5 °C for observation of the exchangeable protons. Chemical shifts for ^1H were referenced to water. Chemical shifts for ^{13}C were not calibrated. Data were processed using TOPSPIN, and the assignments were made using SPARKY.[84] For all NMR experiments, a relaxation delay of 1.5 s was used. Two-dimensional homonuclear NMR spectra were recorded with 512 real data in the t1 dimension and 2048 real data in the t2 dimension. ^1H−^1H NOESY spectra were zero-filled during processing to create a matrix of 1024 × 1024 real points. A skewed sinebell-square apodization with 15° phase shift was used in both dimensions to process ^1H−^1H COSY spectra. The ^1H−^1H TOCSY mixing time was 80 ms. For assignment of exchangeable protons, ^1H−^1H NOESY experiments used the Watergate sequence.[85] The mixing time was 250 ms. For assignment of nonexchangeable protons and the derivation of distance restraints, ^1H−^1H NOESY experiments used TPPI quadrature detection, and mixing times of 60 and 250 ms were used. ^1H−^1H DQF-COSY experiments were performed with TPPI quadrature detection and presaturation of the residual water during the relaxation delay. ^1H−^{13}C HSQC experiments were carried out using standard ^1H-detected pulse programs with States-TPPI phase cycling.[86−88] The spectra were recorded with 256 real data in the t1 dimension and 1024 real data in the t2 dimension and were zero filled to create a matrix of 1024 × 1024 real points. ^1H−^{13}C HMBC experiments used the low phase J-filter to suppress ^1J couplings. The spectra were recorded with 256 real data in the t1 dimension and 1024 real data in the t2 dimension and were zero filled to create a matrix of 1024 × 1024 real points.

Molecular Dynamics. Restrained molecular dynamics (rMD) calculations[51,89] for similar modified oligodeoxynucleotide duplexes have been described.[44,46,90] NOE-derived distances from cross peak volumes measured at mixing 250 ms were calculated using MARDIGRAS.[91] Empirical restraints preserved Watson−Crick hydrogen bonding and prevented propeller twisting between base pairs. The duplex was found to maintain a B-type DNA conformation; except for the cross-linked and the terminal base pairs, the backbone and sugar pucker torsion angle restraints were using empirical data derived from B-DNA.[50] The carbinolamine cross-link was constructed using the program Insight II. The rMD calculations[51,89] were conducted with the AMBER parm99 force field.[92] The generalized Born (GB) model[93] with parameters developed by Tsui and Case[94] was used for implicit water simulation. The program CORMA[51] was utilized to estimate the NOE intensities from the structures refined from rMD calculations. Helicoidal analyses were carried out with 3DNA.[95]

Molecular dynamics simulations in explicit water were performed using the AMBER force field[92] with the particle mesh Ewald[96,97] (PME) method. The refined structure converged from the rMD calculation was used as the starting structure. The cross-link was surrounded by an 8.0 Å cubic TIP3P water box in each direction. A total of 22 Na^+ ions were added to neutralize the duplex. The cutoff radius for nonbonding interactions was 8.0 Å. Bond lengths involving hydrogens were fixed with the SHAKE algorithm. The cross-link was first energy-minimized for 1000 interations. The molecular dynamics simulation was carried out with constant volume at 300 K for 10 000 iterations with an integrator time of 1 fs. The molecular dynamics simulation at constant pressure was performed at 300 K for 5 ns with an integrator time of 1 fs. The PTRAJ module from the AMBER 10 package was used to analyze the trajectories. The rmsd values of the trajectories were referenced to the starting structure. A distance of less than 3.5 Å and an angle of greater than 120° between the potential hydrogen donor and acceptor were used as criteria for hydrogen-bond formation.

■ ASSOCIATED CONTENT

⑤ Supporting Information. Description of the synthesis of isotope-labeled oligodeoxynucleotides; Table S1, chemical shifts of the nonexchangeable protons; Table S2, NOE restraints used for the structural refinement; and Figure S1, HPLC chromatograph of the cross-linked sample; Figure S2, MALDI-TOF mass spectrum of the interstrand cross-link; Figure S3, COSY spectra of the modified duplex before and after cross-linking; Figure S4, NOE connectivities of the base H8/H6 protons with deoxyribose H1′ protons; Figure S5, proton chemical shift perturbations of the cross-link as compared to the related unmodified duplex; Figure S6, assignments of the base exchangeable protons; Figure S7, molecular modeling of the (6S,8R,11S) carbinolamine cross-link **8** and (6S,8R,11S) THF cross-link **11**; Figure S8, force field parameters of the cross-link used for rMD calculations; Figure S9, nucleotide-by-nucleotide sixth root residuals (R_1^x) of the cross-link; Figure S10, refined structures of the interstrand cross-link; Figure S11, backbone torsion angles of the refined structure; Figure S12, ^{31}P NMR of the cross-link **8** as compared to the duplex containing adduct **6**; Figure S13, molecular dynamics simulations in explicit water. This material is available free of charge via the Internet at http://pubs.acs.org.

■ AUTHOR INFORMATION

Corresponding Author
michael.p.stone@vanderbilt.edu

■ REFERENCES

(1) Benedetti, A.; Comporti, M.; Esterbauer, H. *Biochim. Biophys. Acta* **1980**, *620*, 281–296.

(2) Esterbauer, H.; Schaur, R. J.; Zollner, H. *Free Radical Biol. Med.* **1991**, *11*, 81–128.

(3) Burcham, P. C. *Mutagenesis* **1998**, *13*, 287–305.

(4) Lee, S. H.; Blair, I. A. *Chem. Res. Toxicol.* **2000**, *13*, 698–702.

(5) Schneider, C.; Tallman, K. A.; Porter, N. A.; Brash, A. R. *J. Biol. Chem.* **2001**, *276*, 20831–20838.

(6) Schneider, C.; Porter, N. A.; Brash, A. R. *J. Biol. Chem.* **2008**, *283*, 15539–15543.

(7) Parola, M.; Bellomo, G.; Robino, G.; Barrera, G.; Dianzani, M. U. *Antioxid. Redox Signaling* **1999**, *1*, 255–284.

(8) Poli, G.; Schaur, R. J. *IUBMB Life* **2000**, *50*, 315–321.

(9) Nakashima, I.; Liu, W.; Akhand, A. A.; Takeda, K.; Kawamoto, Y.; Kato, M.; Suzuki, H. *Mol. Aspects Med.* **2003**, *24*, 231–238.

(10) West, J. D.; Ji, C.; Duncan, S. T.; Amarnath, V.; Schneider, C.; Rizzo, C. J.; Brash, A. R.; Marnett, L. J. *Chem. Res. Toxicol.* **2004**, *17*, 453–462.

(11) West, J. D.; Marnett, L. J. *Chem. Res. Toxicol.* **2005**, *18*, 1642–1653.

(12) West, J. D.; Marnett, L. J. *Chem. Res. Toxicol.* **2006**, *19*, 173–194.

(13) Dwivedi, S.; Sharma, A.; Patrick, B.; Sharma, R.; Awasthi, Y. C. *Redox Rep.* **2007**, *12*, 4–10.

(14) Sayre, L. M.; Zelasko, D. A.; Harris, P. L.; Perry, G.; Salomon, R. G.; Smith, M. A. *J. Neurochem.* **1997**, *68*, 2092–2097.

(15) Yoritaka, A.; Hattori, N.; Uchida, K.; Tanaka, M.; Stadtman, E. R.; Mizuno, Y. *Proc. Natl. Acad. Sci. U.S.A.* **1996**, *93*, 2696–2701.

(16) Napoli, C.; D'Armiento, F. P.; Mancini, F. P.; Postiglione, A.; Witztum, J. L.; Palumbo, G.; Palinski, W. *J. Clin. Invest.* **1997**, *100*, 2680–2690.

(17) Yamagami, K.; Yamamoto, Y.; Kume, M.; Ishikawa, Y.; Yamaoka, Y.; Hiai, H.; Toyokuni, S. *Antioxid. Redox Signaling* **2000**, *2*, 127–136.

(18) Benamira, M.; Marnett, L. J. *Mutat. Res.* **1992**, *293*, 1–10.

(19) Esterbauer, H.; Eckl, P.; Ortner, A. *Mutat. Res.* **1990**, *238*, 223–233.

(20) Eckl, P. M.; Ortner, A.; Esterbauer, H. *Mutat. Res.* **1993**, *290*, 183–192.

(21) Karlhuber, G. M.; Bauer, H. C.; Eckl, P. M. *Mutat. Res.* **1997**, *381*, 209–216.

(22) Eckl, P. M. *Mol. Aspects Med.* **2003**, *24*, 161–165.

(23) Emerit, I.; Khan, S. H.; Esterbauer, H. *Free Radical Biol. Med.* **1991**, *10*, 371–377.

(24) Chung, F. L.; Komninou, D.; Zhang, L.; Nath, R.; Pan, J.; Amin, S.; Richie, J. *Chem. Res. Toxicol.* **2005**, *18*, 24–27.

(25) Falletti, O.; Cadet, J.; Favier, A.; Douki, T. *Free Radical Biol. Med.* **2007**, *42*, 1258–1269.

(26) Yadav, U. C.; Ramana, K. V.; Awasthi, Y. C.; Srivastava, S. K. *Toxicol. Appl. Pharmacol.* **2008**, *227*, 257–264.

(27) Winter, C. K.; Segall, H. J.; Haddon, W. F. *Cancer Res.* **1986**, *46*, 5682–5686.

(28) Douki, T.; Odin, F.; Caillat, S.; Favier, A.; Cadet, J. *Free Radical Biol. Med.* **2004**, *37*, 62–70.

(29) Kowalczyk, P.; Ciesla, J. M.; Komisarski, M.; Kusmierek, J. T.; Tudek, B. *Mutat. Res.* **2004**, *550*, 33–48.

(30) Yi, P.; Zhan, D.; Samokyszyn, V. M.; Doerge, D. R.; Fu, P. P. *Chem. Res. Toxicol.* **1997**, *10*, 1259–1265.

(31) Chung, F. L.; Nath, R. G.; Ocando, J.; Nishikawa, A.; Zhang, L. *Cancer Res.* **2000**, *60*, 1507–1511.

(32) Wacker, M.; Schuler, D.; Wanek, P.; Eder, E. *Chem. Res. Toxicol.* **2000**, *13*, 1165–1173.

(33) Wacker, M.; Wanek, P.; Eder, E. *Chem.-Biol. Interact.* **2001**, *137*, 269–283.

(34) Chung, F. L.; Zhang, L. *Methods Enzymol.* **2002**, *353*, 523–536.

(35) Liu, X.; Lovell, M. A.; Lynn, B. C. *Chem. Res. Toxicol.* **2006**, *19*, 710–718.

(36) Pan, J.; Davis, W.; Trushin, N.; Amin, S.; Nath, R. G.; Salem, N., Jr.; Chung, F. L. *Anal. Biochem.* **2006**, *348*, 15–23.

(37) Sodum, R. S.; Chung, F. L. *Cancer Res.* **1988**, *48*, 320–323.

(38) Sodum, R. S.; Chung, F. L. *Chem. Res. Toxicol.* **1989**, *2*, 23–28.

(39) Sodum, R. S.; Chung, F. L. *Cancer Res.* **1991**, *51*, 137–143.

(40) Chen, H. J.; Chung, F. L. *Chem. Res. Toxicol.* **1994**, *7*, 857–860.

(41) el Ghissassi, F.; Barbin, A.; Nair, J.; Bartsch, H. *Chem. Res. Toxicol.* **1995**, *8*, 278–283.

(42) Wang, H.; Rizzo, C. J. *Org. Lett.* **2001**, *3*, 3603–3605.

(43) Wang, H.; Kozekov, I. D.; Harris, T. M.; Rizzo, C. J. *J. Am. Chem. Soc.* **2003**, *125*, 5687–5700.

(44) Huang, H.; Wang, H.; Qi, N.; Kozekova, A.; Rizzo, C. J.; Stone, M. P. *J. Am. Chem. Soc.* **2008**, *130*, 10898–10906.

(45) Huang, H.; Wang, H.; Qi, N.; Lloyd, R. S.; Rizzo, C. J.; Stone, M. P. *Biochemistry* **2008**, *47*, 11457–11472.

(46) Huang, H.; Kozekov, I. D.; Kozekova, A.; Wang, H.; Lloyd, R. S.; Rizzo, C. J.; Stone, M. P. *Environ. Mol. Mutagen.* **2010**, *51*, 625–634.

(47) Patel, D. J.; Shapiro, L.; Hare, D. *Q. Rev. Biophys.* **1987**, *20*, 35–112.

(48) Reid, B. R. *Q. Rev. Biophys.* **1987**, *20*, 2–28.

(49) Boelens, R.; Scheek, R. M.; Dijkstra, K.; Kaptein, R. *J. Magn. Reson.* **1985**, *62*, 378–386.

(50) Arnott, S.; Hukins, D. W. L. *Biochem. Biophys. Res. Commun.* **1972**, *47*, 1504–1509.

(51) Borgias, B. A.; James, T. L. *Methods Enzymol.* **1989**, *176*, 169–183.

(52) James, T. L. *Curr. Opin. Struct. Biol.* **1991**, *1*, 1042–1053.

(53) James, T. L. *Methods Enzymol.* **1994**, *239*, 416–439.

(54) Noll, D. M.; Mason, T. M.; Miller, P. S. *Chem. Rev.* **2006**, *106*, 277–301.

(55) Haynes, R. L.; Brune, B.; Townsend, A. J. *Free Radical Biol. Med.* **2001**, *30*, 884–894.

(56) Stone, M. P.; Cho, Y.-J.; Huang, H.; Kim, H.-Y.; Kozekov, I. D.; Kozekova, A.; Wang, H.; Lloyd, R. S.; Harris, T. M.; Rizzo, C. J. *Acc. Chem. Res.* **2008**, *41*, 793–804.

(57) Minko, I. G.; Kozekov, I. D.; Harris, T. M.; Rizzo, C. J.; Lloyd, R. S.; Stone, M. P. *Chem. Res. Toxicol.* **2009**, *22*, 759–778.

(58) Kozekov, I. D.; Nechev, L. V.; Sanchez, A.; Harris, C. M.; Lloyd, R. S.; Harris, T. M. *Chem. Res. Toxicol.* **2001**, *14*, 1482–1485.

(59) Kozekov, I. D.; Nechev, L. V.; Moseley, M. S.; Harris, C. M.; Rizzo, C. J.; Stone, M. P.; Harris, T. M. *J. Am. Chem. Soc.* **2003**, *125*, 50–61.

(60) Kim, H. Y.; Voehler, M.; Harris, T. M.; Stone, M. P. *J. Am. Chem. Soc.* **2002**, *124*, 9324–9325.

(61) Cho, Y. J.; Kim, H. Y.; Huang, H.; Slutsky, A.; Minko, I. G.; Wang, H.; Nechev, L. V.; Kozekov, I. D.; Kozekova, A.; Tamura, P.; Jacob, J.; Voehler, M.; Harris, T. M.; Lloyd, R. S.; Rizzo, C. J.; Stone, M. P. *J. Am. Chem. Soc.* **2005**, *127*, 17686–17696.

(62) Huang, H.; Kim, H. Y.; Kozekov, I. D.; Cho, Y. J.; Wang, H.; Kozekova, A.; Harris, T. M.; Rizzo, C. J.; Stone, M. P. *J. Am. Chem. Soc.* **2009**, *131*, 8416–8424.

(63) Cho, Y. J.; Wang, H.; Kozekov, I. D.; Kurtz, A. J.; Jacob, J.; Voehler, M.; Smith, J.; Harris, T. M.; Lloyd, R. S.; Rizzo, C. J.; Stone, M. P. *Chem. Res. Toxicol.* **2006**, *19*, 195–208.

(64) Cho, Y. J.; Kozekov, I. D.; Harris, T. M.; Rizzo, C. J.; Stone, M. P. *Biochemistry* **2007**, *46*, 2608–2621.

(65) Norman, D.; Live, D.; Sastry, M.; Lipman, R.; Hingerty, B. E.; Tomasz, M.; Broyde, S.; Patel, D. J. *Biochemistry* **1990**, *29*, 2861–2875.

(66) Fagan, P. A.; Spielmann, H. P.; Sigurdsson, S.; Rink, S. M.; Hopkins, P. B.; Wemmer, D. E. *Nucleic Acids Res.* **1996**, *24*, 1566–1573.

(67) Dooley, P. A.; Tsarouhtsis, D.; Korbel, G. A.; Nechev, L. V.; Shearer, J.; Zegar, I. S.; Harris, C. M.; Stone, M. P.; Harris, T. M. *J. Am. Chem. Soc.* **2001**, *123*, 1730–1739.

(68) Dooley, P. A.; Zhang, M.; Korbel, G. A.; Nechev, L. V.; Harris, C. M.; Stone, M. P.; Harris, T. M. *J. Am. Chem. Soc.* **2003**, *125*, 62–72.

(69) Nojima, K.; Hochegger, H.; Saberi, A.; Fukushima, T.; Kikuchi, K.; Yoshimura, M.; Orelli, B. J.; Bishop, D. K.; Hirano, S.; Ohzeki, M.; Ishiai, M.; Yamamoto, K.; Takata, M.; Arakawa, H.; Buerstedde, J. M.; Yamazoe, M.; Kawamoto, T.; Araki, K.; Takahashi, J. A.; Hashimoto, N.; Takeda, S.; Sonoda, E. *Cancer Res.* **2005**, *65*, 11704–11711.

(70) Niedernhofer, L. J.; Lalai, A. S.; Hoeijmakers, J. H. *Cell* **2005**, *123*, 1191–1198.

(71) Mirchandani, K. D.; D'Andrea, A. D. *Exp. Cell Res.* **2006**, *312*, 2647–2653.

(72) Patel, K. J.; Joenje, H. *DNA Repair* **2007**, *6*, 885–890.

(73) Kennedy, R. D.; D'Andrea, A. D. *Genes Dev.* **2005**, *19*, 2925–2940.

(74) Mu, D.; Bessho, T.; Nechev, L. V.; Chen, D. J.; Harris, T. M.; Hearst, J. E.; Sancar, A. *Mol. Cell. Biol.* **2000**, *20*, 2446–2454.

(75) Kumari, A.; Minko, I. G.; Harbut, M. B.; Finkel, S. E.; Goodman, M. F.; Lloyd, R. S. *J. Biol. Chem.* **2008**, *283*, 27433–27437.

(76) Liu, X.; Lao, Y.; Yang, I. Y.; Hecht, S. S.; Moriya, M. *Biochemistry* **2006**, *45*, 12898–12905.

(77) Cole, R. S. *Proc. Natl. Acad. Sci. U.S.A.* **1973**, *70*, 1064–1068.

(78) Berardini, M.; Mackay, W.; Loechler, E. L. *Biochemistry* **1997**, *36*, 3506–3513.

(79) Minko, I. G.; Harbut, M. B.; Kozekov, I. D.; Kozekova, A.; Jakobs, P. M.; Olson, S. B.; Moses, R. E.; Harris, T. M.; Rizzo, C. J.; Lloyd, R. S. *J. Biol. Chem.* **2008**, *283*, 17075–17082.

(80) Chung, F. L.; Pan, J.; Choudhury, S.; Roy, R.; Hu, W.; Tang, M. S. *Mutat. Res.* **2003**, *531*, 25–36.

(81) Feng, Z.; Hu, W.; Amin, S.; Tang, M. S. *Biochemistry* **2003**, *42*, 7848–7854.

(82) Choudhury, S.; Pan, J.; Amin, S.; Chung, F. L.; Roy, R. *Biochemistry* **2004**, *43*, 7514–7521.

(83) Kozekov, I. D.; Turesky, R. J.; Alas, G. R.; Harris, C. M.; Harris, T. M.; Rizzo, C. J. *Chem. Res. Toxicol.* **2010**, *23*, 1701–1713.

(84) Goddard, T. D.; Kneller, D. G. University of California: San Francisco, CA, 2006.

(85) Piotto, M.; Saudek, V.; Sklenar, V. *J. Biomol. NMR* **1992**, *2*, 661–665.

(86) Palmer, A. G., III; Rance, M.; Wright, P. E. *J. Am. Chem. Soc.* **1991**, *113*, 4371–4380.

(87) Kay, L. E.; Keifer, P. A.; Saarinen, T. *J. Am. Chem. Soc.* **1992**, *114*, 10663–10665.

(88) Schleucher, J.; Schwendinger, M.; Sattler, M.; Schmidt, P.; Schedletzky, O.; Glaser, S. J.; Sorensen, O. W.; Griesinger, C. *J. Biomol. NMR* **1994**, *4*, 301–306.

(89) Keepers, J. W.; James, T. L. *J. Magn. Reson.* **1984**, *57*, 404–426.

(90) Huang, H.; Wang, H.; Lloyd, R. S.; Rizzo, C. J.; Stone, M. P. *Chem. Res. Toxicol.* **2009**, *22*, 187–200.

(91) Borgias, B. A.; James, T. L. *J. Magn. Reson.* **1990**, *87*, 475–487.

(92) Case, D. A.; Cheatham, T. E., III; Darden, T.; Gohlke, H.; Luo, R.; Merz, K. M., Jr.; Onufriev, A.; Simmerling, C.; Wang, B.; Woods, R. J. *J. Comput. Chem.* **2005**, *26*, 1668–1688.

(93) Tsui, V.; Case, D. A. *Biopolymers* **2000**, *56*, 275–291.

(94) Ryckaert, J.-P.; Ciccotti, G.; Berendsen, H. J. C. *J. Comput. Phys.* **1977**, *23*, 327–341.

(95) Lu, X. J.; Olson, W. K. *Nucleic Acids Res.* **2003**, *31*, 5108–5121.

(96) Darden, T.; York, D.; Pedersen, L. *J. Chem. Phys.* **1993**, *12*, 10089–10092.

(97) Essmann, U.; Perera, L.; Berkowitz, M. L.; Darden, T.; Lee, H.; Pedersen, L. G. *J. Chem. Phys.* **1995**, *19*, 8577–8593.